Martin K. Schmitt and Hubert Huppertz*

Ni₆B₂₂O₃₉·H₂O – extending the field of nickel borates

https://doi.org/10.1515/znb-2017-0148 Received September 12, 2017; accepted September 20, 2017

Abstract: Ni₆B₂₂O₃₉·H₂O was synthesized in a high-pressure/high-temperature reaction at 5 GPa/900°C. It crystallizes in the orthorhombic space group $Pmn2_1$ (no. 31) with the lattice parameters a=7.664(2), b=8.121(2) and c=17.402(2) Å. The crystal structure is discussed with regard to the isotypic compounds $M_6B_{22}O_{39}\cdot H_2O$ (M=Fe, Co) and the structurally related phase $Cd_6B_{22}O_{39}\cdot H_2O$. Furthermore, the characterization of $Ni_6B_{22}O_{39}\cdot H_2O$ via X-ray powder diffraction and vibrational spectroscopy is reported.

Keywords: crystal structure; high-pressure chemistry; nickel borate; vibrational spectroscopy.

1 Introduction

Owing to their outstanding physical and chemical properties, borates have been the subject of numerous studies in both industry and academia. Their versatile features result from the vast number of different crystal structures borates can adopt, as physical and chemical properties are closely related to the atomic arrangements. The diversity of borates might even exceed that of silicates, as boron can coordinate to three as well as four oxygen atoms.

Most borates were synthesized either at ambient pressure or at only slightly elevated pressures in autoclaves. As the formation of novel compounds requires modified reaction conditions, high-pressure experiments are well suited for the investigation of new materials. The first high-pressure studies on transition metal borates were published by Jansen, Brachtel and Depmeier in the early 1980s [1–4]. By synthesizing β -ZnB $_4$ O $_7$ [5], our group started working on this topic in 2003. Thenceforward, we discovered more than 30 new transition metal borates via high-pressure

Martin K. Schmitt: Institut für Allgemeine, Anorganische und Theoretische Chemie, Universität Innsbruck, Innrain 80–82, 6020 Innsbruck, Austria

experiments. These investigations produced phases with previously unknown compositions (e.g. $M_c B_{22} O_{20} \cdot H_2 O$ (M=Fe, Co, Cd) [6, 7]) or fascinating novel structural motifs (e.g. $Cd(NH_3)_{7}[B_3O_5(NH_3)]_{7}$ [8], the first ammine borate, or Mo₃B₄O₆ [9], the first transition metal cluster containing borate). Furthermore, we observed an impressive diversity of some M-B-O(-H) (M=transition metal) systems. In the system Ni-B-O(-H), for example, only two high-pressure compounds were known until recently, namely high-pressure-NiB₂O₄ [10] and β -NiB₄O₇ [11], which were synthesized at 7.5 GPa/680°C and 7.5 GPa/1150°C, respectively. Recent investigations revealed the existence of three more phases $(\gamma - \text{NiB}_{\lambda} \text{O}_{\tau} [12], \text{Ni}_{\lambda} \text{B}_{\tau} \text{O}_{\tau} (\text{OH})_{\lambda} \cdot \text{H}_{\lambda} \text{O}$ [13] and NiB₃O₅(OH) [14]) within a very narrow p-T range (4–5 GPa/700–900°C), which underlines the potential of high-pressure methods for research focused on the development of new materials.

In this article, we present $Ni_6B_{22}O_{39} \cdot H_2O$, another new nickel borate synthesized at high-pressure conditions. The compound was characterized via X-ray single-crystal and powder diffraction as well as vibrational spectroscopy. The crystal structure of $Ni_6B_{22}O_{39} \cdot H_2O$ will be discussed in the context of the related compounds $M_6B_{22}O_{39} \cdot H_2O$ (M=Fe, Co, Cd) [6, 7].

2 Results and discussion

2.1 Crystal structure

Ni₆B₂₂O₃₉ · H₂O crystallizes in the orthorhombic, acentric space group $Pmn2_1$ (no. 31) with the lattice parameters a = 7.664(2), b = 8.121(2) and c = 17.402(2) Å (Table 1). It is isotypic to the compounds M_6 B₂₂O₃₉ · H₂O (M=Fe, Co) [6] and structurally related to Cd₆B₂₂O₃₉ · H₂O [7]. The latter phase shows a similar crystal structure but crystallizes in the higher symmetric space group Pnma (no. 62).

A comparison of the lattice parameters and cell volumes of the isotypic phases is given in Table 2. All parameters decrease from the iron via the cobalt to the nickel compound. This finding is consistent with the given ionic radii only, if a high-spin configuration is assumed for iron and cobalt. If a low-spin configuration was present, the lattice parameters should evolve conversely.

^{*}Corresponding author: Hubert Huppertz, Institut für Allgemeine, Anorganische und Theoretische Chemie, Universität Innsbruck, Innrain 80–82, 6020 Innsbruck, Austria, Fax: +43 (512) 507-57099, E-mail: Hubert.Huppertz@uibk.ac.at

Table 1: Crystal and structure refinement data for $Ni_6B_{22}O_{39} \cdot H_2O$.

Molar mass, $g \cdot mol^{-1}$ 12 Crystal system Or	$_{6}B_{22}O_{39} \cdot H_{2}O$ 232.10 rthorhombic $mn2_{1}$ (no. 31)
Crystal system Or	rthorhombic mn2 ₁ (no. 31)
, ,	mn2 ₁ (no. 31)
Space group Pn	•
	- (0)
Single-crystal data	(0)
<i>T</i> , °C 24	4(2)
Radiation; λ, Å Mo	ο <i>K_α</i> ; 0.71073
a, Å 7.6	664(2)
b, Å 8.3	121(2)
c, Å 17	7.402(2)
<i>V</i> , Å ³	083.1(2)
<i>Z</i> 2	
Calculated density, g·cm ⁻³ 3.7	78
Absorption coeff., mm ⁻¹ 5.3	3
F(000), e 12	200
Crystal size, mm ³ 0.3	$10 \times 0.06 \times 0.06$
θ Range, deg 2.3	34-37.82
Range in <i>hkl</i> -1	$11 \le h \le 13, -13 \le k \le 14,$
-2	22≤1≤29
Reflections collected 14	4555
Independent reflections 54	491 [R _{int} =0.039]
	9.9
Refinement method Fu	ıll-matrix least-squares on <i>F</i> 2
Data/restraints/parameters 54	491/2/338
Goodness-of-fit on F^2 1.0	056
Final $R1/wR2$ [$I > 2\sigma(I)$] 0.0	037/0.082
Final R1/wR2 (all data) 0.0	042/0.085
Flack parameter (x) 0.0	01(1)
Largest diff. peak/hole, e Å ⁻³ 0.7	78/-1.90
Powder data	
Radiation; λ, Å Mo	$oK_{\alpha 1}$; 0.7093
a, Å 7.6	6594(3)
,	1161(4)
c, Å 17	7.3930(7)
<i>V</i> , Å ³ 10	081.22(7)
2θ Range, deg 2.0	0-46.4
2θ Step width, deg 0.0	015
$R_{\rm exp}$, %	03
R_{wp} , %	12
$R_{\rm p}$, %	66

The crystal structure of Ni₆B₂₂O₃₉·H₂O consists of vertex-sharing [BO₄] tetrahedra and non-planar, pyramidal [BO₃] groups forming corrugated layers parallel to (001).

These layers are interconnected along [001] through $[BO_4]$ tetrahedra centered by the boron atom B11 (Fig. 1; light blue tetrahedra). The nickel atoms are located in the channels between the borate layers.

Similar to $M_6B_{22}O_{30} \cdot H_2O$ (M=Fe, Co), $Ni_6B_{22}O_{30} \cdot H_2O$ shows a structural feature that can be considered as an intermediate state between a planar [BO₃] and a tetrahedral [BO₄] group (Fig. 2a). In the nickel compound, however, the non-planar [BO₃] group involves the atom B8, whereas the corresponding arrangement is observed for B11 in $M_{\bullet}B_{\circ}O_{\circ} \cdot H_{\bullet}O$ (M=Fe, Co) (Fig. 2). Interestingly, the boron site B6 in Cd₆B₂O₃₉·H₂O that corresponds to the B11 site (there are less independent atom sites due to the higher symmetry of the cadmium phase, hence the atom names differ) shows a nearly trigonal planar configuration. Apparently, the coordination environments of B8 and B11 change depending on the radius of the transition metal. An increasing radius promotes a shift towards a (more regular) tetrahedral coordination of B8 and, at the same time, a trigonal planar coordination of B11 (Fig. 2 and Table 3).

The individual B–O bond lengths of the tetrahedrally coordinated boron sites (B1–B7 and B9–B11) range from 1.402(4) to 1.611(5) Å (Table 4) with an average value of 1.479 Å, which is in accordance with the literature value (1.476(35) Å) [16]. The corresponding B–O distances in the non-planar [BO₃] group (B8) are 1.416(5)–1.454(5) Å (average: 1.430 Å). Similar to $M_6B_{22}O_{39} \cdot H_2O$ (M=Fe, Co), the mean value is significantly larger compared to planar [BO₃] groups (1.370(19) Å) [17].

There are six crystallographically distinguishable nickel sites in $Ni_6B_{22}O_{39} \cdot H_2O$. Four are coordinated octahedrally [coordination number (CN) 6; Ni1, Ni3–5], Ni2 shows a monocapped tetrahedral coordination (CN 4+1), and Ni6 is coordinated in the form of a trigonal bipyramid (CN 5) (Fig. 3). These coordination environments match those observed in $M_6B_{22}O_{39} \cdot H_2O$ (M=Fe, Co) except for Ni6. In the latter compounds, the corresponding M6 position shows a 4+1 coordination like M2. The reason for this structural deviation is the difference between the two longest M6-O bonds, which is much larger in the iron and cobalt phases compared to the nickel compound (Table 5).

Table 2: Comparison of the lattice parameters (Å), volumes (ų) and ionic radii (for CN 6) (Å) [15] of Ni₆B₂₂O₃₉ · H₂O and M_6 B₂₂O₃₉ · H₂O (M = Fe, Co) [6].

Compound	а	b	с	V	r(M²+)
Fe ₆ B ₂₂ O ₃₉ ·H ₂ O Co ₆ B ₂₂ O ₃₉ ·H ₂ O	7.719(2) 7.701(2)	8.234(2) 8.176(2)	17.680(4) 17.469(4)	1123.7(4) 1099.9(4)	0.75 (l.s.)/0.920 (h.s.) 0.79 (l.s.)/0.885 (h.s.)
$Ni_6B_{22}O_{39} \cdot H_2O$	7.664(2)	8.121(2)	17.402(2)	1083.1(2)	0.830

al.s., Low spin; h.s., high spin.

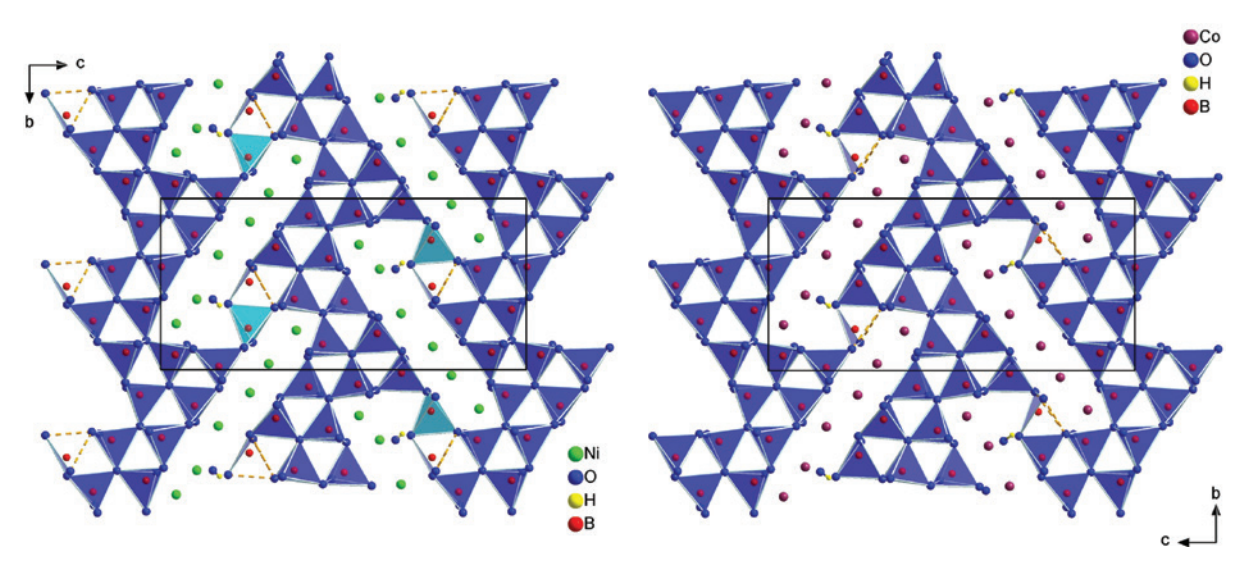


Fig. 1: Left: crystal structure of $Ni_aB_{27}O_{39} \cdot H_2O$. The corrugated layers consisting of $[BO_a]$ tetrahedra and non-planar $[BO_3]$ groups are interconnected along [001] through [BO] tetrahedra (light blue). Right: crystal structure of Co, B, 0, + H, 0. Here, the corrugated layers are interconnected via non-planar, pyramidal [BO,] groups. The orientation of both crystal structures is different as the atomic coordinates of Ni₂B₂,O₃₀ · H₂O had to be inverted during the refinement (see Experimental Section for more details).

To our knowledge, a trigonal bipyramidal coordination of nickel through oxygen was observed only rarely in solid state chemistry. The compound (Mg_{1.55}Ni_{0.45})(OH)(AsO₄), for example, exhibits a trigonal bipyramidally coordinated magnesium site, which is also partially (~4%) occupied by nickel.

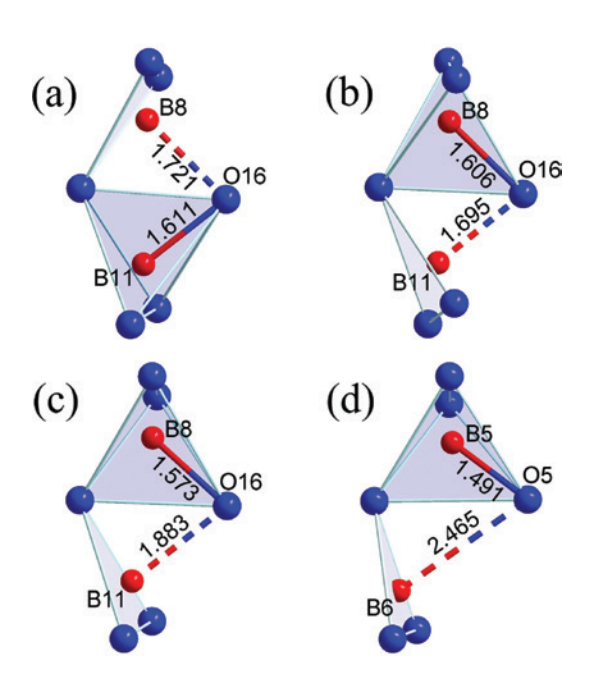


Fig. 2: Comparison of the coordination environments of B8 and B11 (and their analogs B5 and B6 in the cadmium phase) in $M_6 B_{22} O_{39} \cdot H_2 O_{39} \cdot H_2 O_{39} \cdot H_3 O_{39$ in (Å) (see also Table 3).

Table 6 shows the Ni–O bond lengths in Ni₆B₂₂O₃₉ · H₂O. The bond lengths of the octahedrally coordinated nickel atoms vary between 1.995(3) and 2.390(4) Å, which is a larger range compared to other high-pressure nickel borates (e.g. $Ni_3B_{18}O_{28}(OH)_4 \cdot H_2O$: 2.064(2)–2.184(3) Å [13] or NiB₃O₅(OH): 1.998(2)–2.171(2) Å [14]), but similar to the distances observed in $Na_{2}Ni_{2}B_{12}O_{21}$ (1.97(1)–2.33(1) Å) [18]. The Ni-O distances of the sites Ni2 (CN 4+1) and Ni6 (CN 5) lie between 1.925(4) and 2.356(4) Å. Compared to Ni-O bond lengths in [NiO₄] tetrahedra (NiCr₂O₄: 1.969 Å [19]) or $[NiO_s]$ square pyramids (β -NiB_{δ}O_s: 2.001(2)–2.060(4) Å [11]), the observed values spread over a larger range. The displacement ellipsoids of Ni2 and Ni6 show a more anisotropic shape than those of the remaining nickel atoms (Fig. 3 and Table 7), which can be related to the different coordination geometries of these nickel sites. The positions of the ligands and the corresponding bond lengths

Table 3: Selected B-O distances and ionic radii (for CN 6) (Å) (see also Fig. 2). For comparison, the average bond lengths (Ø) calculated from the remaining B-O distances of the corresponding coordination environment (i.e. without B-O16) are shown as well.a

Compound	B8-016	ØB8-0	B11-016	ØB11-0	r(M ²⁺)
Ni ₆ B ₂₂ O ₃₉ · H ₂ O	1.721(5)	1.430	1.611(5)	1.469	0.830
$Co_6B_{22}O_{39} \cdot H_2O$	1.606(4)	1.448	1.695(4)	1.457	0.885 (h.s.)
$Fe_{6}B_{22}O_{39} \cdot H_{2}O$	1.573(5)	1.453	1.882(6)	1.461	0.920 (h.s.)
$Cd_{6}B_{22}O_{39} \cdot H_{2}O^{b}$	1.491(4)	1.475	2.465(7)	1.430	1.09

 a h.s., High spin; b B8 ↔ B5, B11 ↔ B6 and O16 ↔ O5 in Cd₆B₂₂O₃₉ · H₂O.

Table 4: Interatomic B–O distances (Å) for Ni₆B₂₂O₂₀ · H₂O.

Ø	1.469	Ø	1.482	Ø	1.505		
-021	1.527(5)	-022	1.529(5)	-016	1.611(5)		
-08	1.454(5)	-016	1.507(5)	-015	1.499(5)		
-05	1.449(4)	-021	1.490(4)	-024	1.492(4)		
B9-03	1.447(5)	B10-026	1.402(4)	B11-02	1.416(5)		
Ø	1.463	Ø	1.465	Ø	1.477	-016	1.721(5)
-020	1.483(4)	-022	1.495(4)	-020	1.546(5)	Ø	1.430
-021	1.477(5)	-019	1.474(5)	-03	1.464(5)	-015	1.454(5)
-012	1.447(5)	-07	1.456(4)	-018	1.453(4)	-04	1.419(4)
B5-09	1.444(4)	B6-018	1.435(5)	B7-011	1.443(4)	B8-08	1.416(5)
Ø	1.478	Ø	1.488	Ø	1.484	Ø	1.481
-019	1.544(5)	-02	1.508(5)	-022	1.574(5)	-020	1.549(4)
-013	1.465(4)	-06	1.498(4)	-01	1.459(5)	-019	1.484(4)
-014	1.455(5)	-014	1.477(5)	-012	1.455(4)	-023	1.449(4)
B1-01	1.446(5)	B2-010	1.467(5)	B3-017	1.448(4)	B4-010	1.441(5)

Average values in bold characters.

are relatively homogenously distributed for the octahedrally coordinated nickel sites. As Ni2 and Ni6 exhibit a less balanced coordination sphere, a stronger anisotropic displacement of these atoms can be observed whereby the

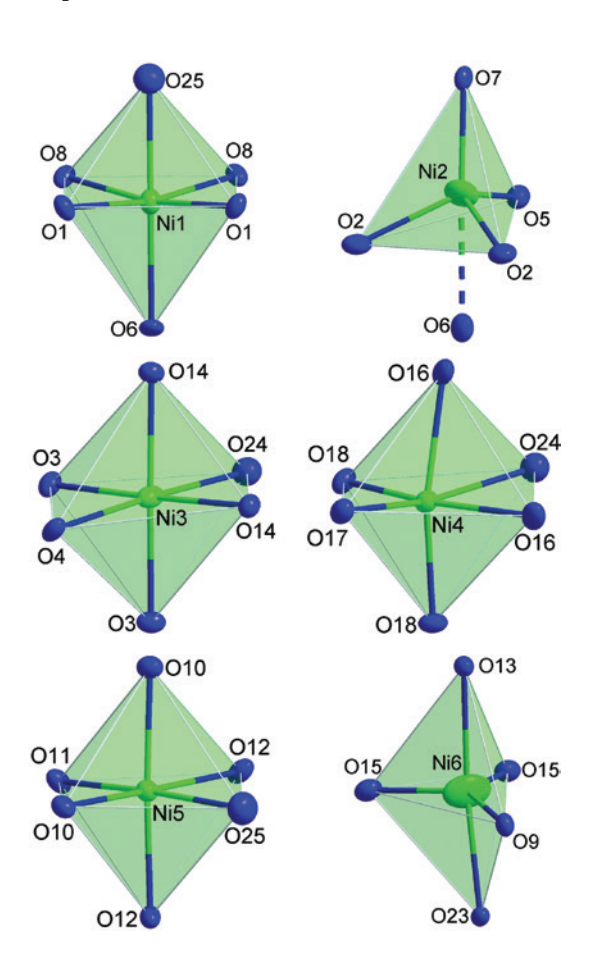


Fig. 3: Coordination environments of the six crystallographically different nickel atoms. All atoms are drawn as displacement ellipsoids at the 90% probability level.

strongest displacement occurs in directions where existing bonds have to be stretched or compressed as little as possible. This effect is more pronounced for Ni6, as the bond lengths (and hence the bond strengths) towards the equatorial and apical oxygen atoms differ significantly (Table 6).

The water molecule in $Ni_6B_{22}O_{39} \cdot H_2O$ is built up by the atoms O25 and H1. A strong hydrogen bond is formed towards O15, which connects the non-planar $[BO_3]$ group and the adjacent $[BO_4]$ tetrahedron, and a weaker one towards O2 (Fig. 4 and Table 8). Atom O25 does not coordinate to any boron atom. Apart from the hydrogen atoms, it only interacts with Ni1 and Ni5.

Bond valence sums were calculated according to the bond-length/bond-strength (BLBS) concept (Table 9) [20, 21]. Within the limits of this concept, the calculated values correspond to the expected formal ionic charges. The "undersaturation" of the transition metal sites M1-M3 and M6 were also observed in $M_6B_{22}O_{39} \cdot H_2O$ (M=Fe, Co) [6], albeit to a lesser extent. The positional parameters of Ni₆B₂₂O₃₉ · H₂O are given in Table 10.

Further details of the crystal structure investigation may be obtained from FIZ Karlsruhe, 76344 Eggenstein-Leopoldshafen, Germany (fax: +49-7247-808-666; e-mail: crysdata@fiz-karlsruhe.de) on quoting the deposition number CSD-433578 for Ni₆B₂,O₃₀·H₂O.

Table 5: Comparison of selected M6-O (M=Fe, Co, Ni) distances (Å).

Compound	M6-013	M6-023	Difference
$\overline{Fe_{6}B_{22}O_{39}\cdotH_{2}O}$	2.141(4)	2.609(3)	0.468
$Co_6B_{22}O_{39} \cdot H_2O$	2.129(3)	2.521(3)	0.392
$Ni_6B_{22}O_{39} \cdot H_2O$	2.311(4)	2.225(4)	-0.086

Table 6: Interatomic Ni–O distances (Å) in Ni $_6$ B $_{22}$ O $_{39}$ · H $_2$ O.

Ø	2.059		Ø	2.066		Ø	2.088	
-024	2.158(4)		-025	2.088(4)		-013	2.311(4)	
-016	2.104(3)	2×	-011	2.073(4)		-023	2.225(4)	
-017	1.997(4)		-012	2.068(3)	2×	-015	1.989(3)	$2\times$
Ni4-018	1.995(3)	2×	Ni5-010	2.050(3)	2×	Ni6-09	1.925(4)	
Ø	2.111		Ø	2.081		Ø	2.153	
-06	2.175(3)		-06	2.356(4)		-024	2.390(4)	
-08	2.148(3)	2×	-02	2.024(3)	2×	-04	2.209(4)	
-025	2.127(4)		-07	2.007(4)		-03	2.084(3)	$2 \times$
Ni1-01	2.034(3)	2×	Ni2-05	1.995(4)		Ni3-014	2.075(3)	$2\times$

Average values in bold characters.

Table 7: Anisotropic displacement parameters U_{ij} (Ų) for $Ni_6B_{22}O_{39} \cdot H_2O$.

U ₂₃	U ₁₃	U ₁₂	U ₃₃	U ₂₂	U ₁₁	Atom
-0.0007(2)	0	0	0.0054(2)	0.0080(2)	0.0053(3)	Ni1
-0.0031(2)	0	0	0.0075(3)	0.0115(3)	0.0160(3)	Ni2
-0.0005(2)	0	0	0.0049(2)	0.0111(3)	0.0057(3)	Ni3
-0.0004(2)	0	0	0.0058(2)	0.0060(2)	0.0048(3)	Ni4
-0.0001(2)	0	0	0.0052(2)	0.0057(2)	0.0051(3)	Ni5
-0.0008(2)	0	0	0.0037(3)	0.0156(3)	0.0326(5)	Ni6
0.000(2)	-0.000(2)	0.000(2)	0.007(2)	0.005(2)	0.005(2)	B1
-0.000(2)	-0.000(2)	0.000(2)	0.004(2)	0.006(2)	0.007(2)	B2
0.001(2)	-0.000(2)	0.001(2)	0.005(2)	0.007(2)	0.004(2)	B3
0.001(2)	0.001(2)	-0.000(2)	0.003(2)	0.005(2)	0.007(2)	B4
0.001(2)	-0.001(2)	0.001(2)	0.004(2)	0.005(2)	0.009(2)	B5
0.001(2)	0.000(2)	-0.001(1)	0.004(2)	0.007(2)	0.005(2)	B6
0.001(2)	-0.002(2)	-0.001(2)	0.007(2)	0.003(2)	0.006(2)	B7
-0.004(2)	-0.001(2)	0.001(2)	0.012(2)	0.010(2)	0.008(2)	B8
-0.001(2)	0.000(2)	-0.000(2)	0.004(2)	0.007(2)	0.007(2)	B9
0.000(2)	-0.002(2)	0.000(2)	0.005(2)	0.008(2)	0.006(2)	B10
-0.002(2)	-0.002(2)	0.001(2)	0.012(2)	0.010(2)	0.008(2)	B11
0.0000(8)	-0.0003(8)	-0.0022(8)	0.0056(9)	0.0079(9)	0.005(2)	01
0.0024(8)	-0.0001(8)	0.0008(9)	0.0061(9)	0.009(2)	0.011(2)	02
-0.0019(8)	0.0005(8)	-0.0020(8)	0.005(1)	0.0072(9)	0.006(2)	03
-0.000(2)	0	0	0.010(2)	0.005(2)	0.004(2)	04
0.001(2)	0	0	0.008(2)	0.008(2)	0.007(2)	05
0.002(2)	0	0	0.010(2)	0.004(2)	0.008(2)	06
0.001(2)	0	0	0.008(2)	0.006(2)	0.004(2)	07
-0.0022(8)	-0.0013(8)	0.0012(7)	0.0047(9)	0.0062(9)	0.006(2)	08
0.000(2)	0	0	0.006(2)	0.007(2)	0.004(2)	09
0.0011(8)	0.0009(8)	0.0004(7)	0.006(2)	0.0067(9)	0.006(2)	010
-0.002(2)	0	0	0.004(2)	0.009(2)	0.005(2)	011
0.0005(8)	0.0028(8)	0.0005(7)	0.008(2)	0.0047(8)	0.007(2)	012
-0.000(2)	0	0	0.007(2)	0.005(2)	0.005(2)	013
-0.0001(8)	-0.0003(8)	0.0012(7)	0.006(2)	0.0070(9)	0.006(2)	014
-0.0018(8)	-0.0006(8)	0.0006(8)	0.007(2)	0.0071(9)	0.010(2)	015
-0.0017(8)	0.0008(8)	0.0012(8)	0.005(2)	0.012(2)	0.006(2)	016
-0.002(2)	0	0	0.006(2)	0.009(2)	0.006(2)	017
0.0000(8)	0.0017(8)	-0.0005(8)	0.008(2)	0.0054(9)	0.005(2)	018
0.0007(7)	0.0006(7)	0.0001(7)	0.0035(9)	0.0051(8)	0.007(2)	019
0.0011(8)	-0.0005(8)	-0.0005(7)	0.0044(9)	0.0057(9)	0.005(2)	020
-0.0003(7)	0.0000(8)	-0.0011(7)	0.0042(9)	0.0036(8)	0.009(2)	021
-0.0005(7)	0.0008(8)	0.0003(7)	0.0038(9)	0.0041(8)	0.007(2)	022
-0.002(2)	0	0	0.007(2)	0.006(2)	0.004(2)	023
-0.001(2)	0	0	0.009(2)	0.010(2)	0.009(2)	024
-0.002(2)	0	0	0.009(2)	0.011(2)	0.012(2)	025
0.000(2)	0	0	0.005(2)	0.009(2)	0.005(2)	026

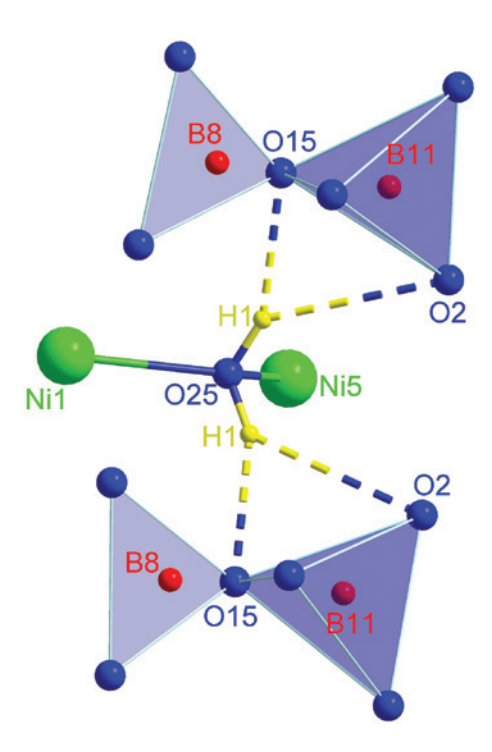


Fig. 4: Hydrogen bonds in Ni₆B $_{22}$ O $_{39} \cdot$ H $_2$ O. *D*-H bonds are drawn as solid lines, H \cdots A bonds as dashed lines.

Table 8: Hydrogen bond lengths (Å) and angles (deg) for $Ni_8B_{22}O_{30}\cdot H_2O.^a$

<i>D</i> –H··· <i>A</i>	d(D-H)	<i>d</i> (H ⋅ ⋅ ⋅ <i>A</i>)	$d(D\cdots A)$	∡(DHA)
025-H1···02_\$6	0.84(3)	2.43(8)	3.099(5)	137(10)
025-H1···015	0.84(3)	1.86(5)	2.645(3)	155(11)

aSymmetry transformations used to generate equivalent atoms: \$6: -x+3/2, -y+1, z+1/2.

2.2 X-ray powder diffraction

Figure 5 displays the result of the Rietveld refinement. Apart from an amorphous phase, which is indicated by

Table 9: Bond valence sums in $Ni_6B_{22}O_{30} \cdot H_2O$ according to BLBS.

Ni1 1.76	Ni2 1.67	Ni3 1.63	Ni4 2.04	Ni5 1.97	Ni6 1.67		H1 1.15				
B1	B2	B3	B4	B5	B6	B7	B8 ^[3]	B8 ^[4]	B9	B10	B11
3.01	2.92	2.98	2.99	3.13	3.11	3.02	2.56	2.95	3.08	2.99	2.84
01	02	03	04	05	06	07	08	09	010	011	012
-1.97	-2.09	-1.91	-1.98	-2.02	-1.81	-1.97	-1.95	-2.13	-1.94	-1.97	-1.94
013	014	015	016	017	018	019	020	021	022	023	024
-1.72	-1.87	-2.16	-1.90	-2.02	-2.04	-2.12	-1.98	-2.13	-1.94	-1.83	-1.84
025 -2.10	026 -1.84										

Superscript numbers in square brackets indicate the number of ligands used for the calculation.

the halo at low 2θ angles, the reaction product consisted primarily of $\text{Ni}_6\text{B}_{22}\text{O}_{39}\cdot\text{H}_2\text{O}$ (~52 wt%) and $\text{NiB}_3\text{O}_5(\text{OH})$ [14] (~48 wt%). Only few minor peaks could not be ascribed to any known phase. More details concerning the refinement are given in Table 1.

2.3 Vibrational spectroscopy

The IR and Raman spectra of a single-crystal are shown in Fig. 6. Between approximately 3600 and 2900 cm⁻¹, the stretching vibrations of the water molecule can be seen in the IR spectrum [22]. The origin of the broad peak at 2000 cm⁻¹ is uncertain, whereas the band at ~1450 cm⁻¹ can presumably be ascribed to stretching vibrations of the (non-planar) [BO₃] group [23]. Below ~1300 cm⁻¹, the IR spectrum is poorly resolved and allows no band assignment.

As the Raman spectrum exhibited strong fluorescence effects above \sim 1500 cm⁻¹, only the lower part of the spectrum is shown. Stretching vibrations of [BO₄] tetrahedra can be observed between 1200 and 900 cm⁻¹, while bending and complex vibrations of both [BO₃] and [BO₄] groups give rise to bands in the wavenumber region \sim 900–200 cm⁻¹ [24, 25]. Lattice vibrations which involve the nickel atoms occur below approximately 350 cm⁻¹ [12].

3 Conclusions

The crystal structure of $Ni_6B_{22}O_{39} \cdot H_2O$ is isotypic to $M_6B_{22}O_{39} \cdot H_2O$ (M=Fe, Co) [6] and related to $Cd_6B_{22}O_{39} \cdot H_2O$ [7]. It consists of corrugated layers parallel to (001) which are composed of corner-linked [BO₃] and [BO₄] groups. Some borate units in $Ni_6B_{22}O_{39} \cdot H_2O$ exhibit a structural arrangement that can be considered as intermediate between a flat [BO₃] triangle and a

Table 10: Atomic coordinates and equivalent isotropic displacement parameters U_{eq} in Å² (U_{iso} for H1) for Ni₆B₂₂O₃₉ · H₂O.

Atom	Wyckoff position	х	у	Z	$U_{\rm eq}/U_{\rm iso}$
Ni1	2 <i>a</i>	1/2	0.67122(8)	0.65767(4)	0.0063(2)
Ni2	2 <i>a</i>	0	0.96616(9)	0.29545(4)	0.0117(2)
Ni3	2 <i>a</i>	0	0.86515(9)	0.74445(4)	0.0073(2)
Ni4	2 <i>a</i>	0	0.22948(8)	0.87094(4)	0.0055(2)
Ni5	2 <i>a</i>	1/2	0.26879(7)	0.54253(4)	0.0054(2)
Ni6	2 <i>a</i>	0	0.4113(2)	0.59893(4)	0.0173(2)
B1	4 <i>b</i>	0.8362(5)	0.7885(5)	0.5923(2)	0.0056(6)
B2	4 <i>b</i>	0.6742(5)	0.0195(4)	0.6585(2)	0.0059(5)
B3	4 <i>b</i>	0.6678(5)	0.6016(4)	0.5020(2)	0.0053(6)
B4	2 <i>a</i>	0.8358(5)	0.0871(4)	0.5395(2)	0.0047(5)
B5	2 <i>a</i>	0.8308(6)	0.3513(4)	0.4600(2)	0.0059(6)
B6	2 <i>a</i>	0.6644(5)	0.1479(5)	0.9426(2)	0.0054(6)
B7	2 <i>a</i>	0.6656(5)	0.1012(4)	0.4049(2)	0.0055(6)
B8	4 <i>b</i>	0.8373(5)	0.5130(5)	0.7427(3)	0.0099(6)
B9	2 <i>a</i>	0.6701(5)	0.7152(5)	0.8147(2)	0.0058(6)
B10	4 <i>b</i>	0.8380(5)	0.5884(4)	0.3655(2)	0.0064(6)
B11	2 <i>a</i>	0.8285(5)	0.2420(5)	0.7394(3)	0.0099(6)
01	4 <i>b</i>	0.6916(3)	0.6790(3)	0.5769(2)	0.0063(4)
02	2 <i>a</i>	0.8099(4)	0.8710(3)	0.2281(2)	0.0087(4)
03	4 <i>b</i>	0.8052(3)	0.8369(3)	0.8270(2)	0.0062(4)
04	4 <i>b</i>	0	0.5937(4)	0.7526(2)	0.0064(6)
05	4 <i>b</i>	0	0.2072(5)	0.3176(2)	0.0073(6)
06	2 <i>a</i>	1/2	0.9382(4)	0.6676(2)	0.0069(6)
07	4 <i>b</i>	0	0.8961(4)	0.4061(2)	0.0057(6)
08	4 <i>b</i>	0.6921(3)	0.6206(3)	0.7444(2)	0.0056(4)
09	4 <i>b</i>	0	0.4002(4)	0.4884(2)	0.0058(6)
010	4 <i>b</i>	0.6893(3)	0.1208(3)	0.5890(2)	0.0061(4)
011	4 <i>b</i>	1/2	0.1501(4)	0.4371(2)	0.0060(6)
012	2 <i>a</i>	0.6980(3)	0.4252(3)	0.5080(2)	0.0066(4)
013	2 <i>a</i>	0	0.6957(4)	0.5952(2)	0.0057(6)
014	2 <i>a</i>	0.8115(3)	0.8919(3)	0.6598(2)	0.0061(4)
015	4 <i>b</i>	0.8304(4)	0.3845(3)	0.6846(2)	0.0078(4)
016	2 <i>a</i>	0.8077(4)	0.3640(3)	0.8118(2)	0.0077(5)
017	4 <i>b</i>	0 04 02(2)	0.3607(4)	0.9680(2)	0.0067(6)
018	4 <i>b</i>	0.8103(3)	0.0762(3)	0.9033(2)	0.0062(4)
019	4 <i>b</i>	0.8375(3)	0.9078(3)	0.5233(2) 0.4606(2)	0.0053(4)
020	4 <i>b</i>	0.8049(3)	0.1703(3)		0.0052(4)
021	4 <i>b</i>	0.8119(4)	0.4093(3)	0.3800(2)	0.0055(4)
022	4b	0.8068(3)	0.6700(3)	0.4435(2)	0.0049(4)
023	4 <i>b</i>	0	0.1438(4)	0.5712(2)	0.0056(6)
024	4b 4b	0	0.1591(5)	0.7514(2)	0.0092(6)
025 026		1/2	0.4113(5)	0.6424(2)	0.0107(7) 0.0061(6)
	4 <i>b</i>	0 503(6)	0.6266(4)	0.3327(2)	
H1	4 <i>b</i>	0.593(8)	0.38(2)	0.661(5)	0.10(4)

 $U_{\rm eq}$ is defined as one third of the trace of the orthogonalized $U_{\rm ii}$ tensor.

 $[BO_{4}]$ tetrahedron. The phases $M_{6}B_{22}O_{39} \cdot H_{2}O$ (M = Fe, Co) show this feature as well, but the respective coordination environments (CN 3+1 vs. CN 4) of the boron sites B8 and B11 are interchanged compared to Ni₆B₂₂O₃₉ · H₂O. Of the six crystallographically different nickel atoms, four are coordinated octahedrally, one exhibits a trigonal

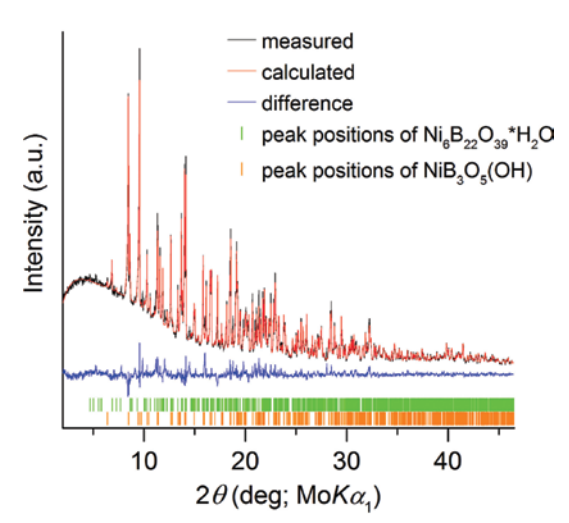


Fig. 5: Rietveld refinement plot.

bipyramidal coordination and one is coordinated in the form of a monocapped tetrahedron.

By synthesizing Ni₂B₂₂O₂₀·H₂O, we added a further phase to the already rich field of high-pressure nickel borates. The high-pressure/high-temperature reaction was carried out at 5 GPa/900°C, which are the same conditions used for the synthesis of γ -NiB, O_{τ} [12]. One of the main differences between both syntheses is the employed crucible material (note that the Ni:B ratio was 1:4 in both cases; see Experimental Section). While γ -NiB, O_{τ} was synthesized in an α -BN crucible, the synthesis of Ni₆B₂O₃₉·H₂O was performed using a molybdenum capsule. The fact that two more phases were synthesized at quite similar reaction conditions $(Ni_3B_{18}O_{28}(OH)_4 \cdot H_2O [13]: 5 GPa/700°C and$ NiB₃O₅(OH) [14] 4 GPa/750°C) emphasizes the impressive diversity of the system Ni-B-O-(H), which we will continue to explore in future experiments.

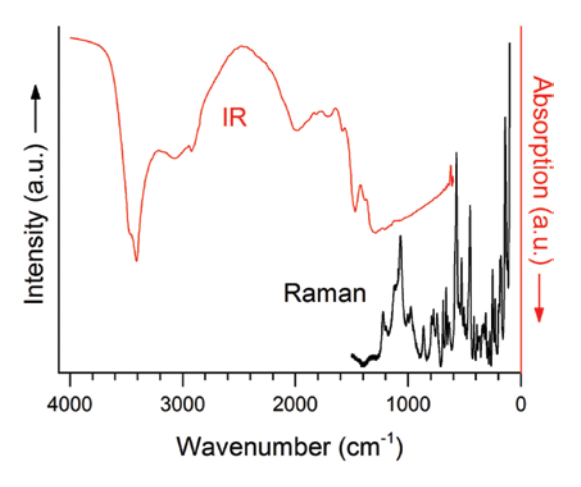


Fig. 6: Single-crystal IR (red) and Raman (black) spectrum of $Ni_6B_{22}O_{39} \cdot H_2O.$

4 Experimental section

4.1 Synthesis

high-pressure/high-temperature synthesis 5 GPa/900°C was carried out in a Walker-type multianvil apparatus in combination with a 1000 t press (both Max Voggenreiter GmbH, Germany). A 1:2 molar mixture of NiO (Avocado Research Chemicals, UK, 99.5%) and B₂O₂ (Strem Chemicals, USA, 99.9+%) was used as starting material. The reactants were weighed and ground in an agate mortar under ambient conditions, which led to a partial hydrolysis of B₂O₃. The starting mixture was then encapsulated in molybdenum foil before it was placed in a crucible, which was closed with a lid (both made of α -BN; Henze Boron Nitride Products AG, Germany). The synthesis was performed using an 18/11 assembly, which was compressed via a two-step mechanism. A more detailed description of the experimental setup can be found in the literature [26-28].

The high-pressure synthesis comprised several steps: first, the sample was compressed to 5 GPa over 125 min. It was then heated to 900°C within 10 min and exposed to this temperature for 100 min. Subsequently, the temperature was reduced to 550°C over 50 min before the heating was switched off to quench the sample to room temperature. Finally, the pressure was released within 12 h. The reaction product consisted of light green (NiB,O,(OH) [14]) and dichroic (purple \leftrightarrow dark green; Ni₆B₂₂O₃₉ · H₂O) crystals. A similar dichroism (red \leftrightarrow bluish) was also observed for $Co_6B_{22}O_{39} \cdot H_2O$ [6].

Ni₆B₂₂O₃₉·H₂O also occurred in a reaction at 6 GPa/1000°C using a reagent mixture in the correct stoichiometry. However, besides Ni₆B₂₂O₃₉·H₂O the reaction product contained also γ -NiB, O_{τ} [12] and at least one unknown compound. Further attempts to synthesize a phase pure sample of Ni₆B₂₂O₃₀ · H₂O failed.

4.2 Single-crystal structure analysis

The single-crystal diffraction data were obtained using a Nonius Kappa-CCD diffractometer with graphitemonochromatized Mo K_{α} radiation ($\lambda = 0.7107$ Å). The data set was corrected for absorption effects employing a semiempirical approach based on equivalent and redundant intensities (Scalepack [29]). The crystal structure was refined with SHELXL [30] (version 2016/6) as implemented in Wingx [31] (version 2013/3) starting from the structural model of the isotypic compound $Co_6B_{22}O_{39} \cdot H_2O$ [6]. As this model corresponded to the wrong twin domain, all atomic coordinates were inverted which led to a Flack parameter of x = 0.01(1) (calculated according to Parsons et al. [32] based on 1923 intensity quotients). All non-hydrogen atoms were refined using anisotropic displacement parameters. A restraint was applied for the distance O25-H1. More details on the data collection and structure refinement are presented in Table 1.

4.3 X-ray powder diffraction

A powdered sample of the reaction product was analyzed using a Stoe Stadi P powder diffractometer equipped with a Dectris Mythen 1K detector. The measurement was carried out in transmission geometry with Ge(111)-monochromatized Mo K_{c1} radiation ($\lambda = 0.7093$ Å). Topas 4.2 [33] was used for the Rietveld refinement. More details are provided in Table 1.

4.4 Vibrational spectroscopy

A Bruker Vertex 70 FT-IR spectrometer (spectral resolution 4 cm⁻¹) equipped with a Globar mid-IR source and a KBr beam splitter was used to acquire the single-crystal absorption spectrum in the wavenumber range 600-4000 cm⁻¹. The spectrometer was attached to a Bruker Hyperion 3000 microscope and equipped with a mercury cadmium telluride (MCT) detector. Three hundred and twenty scans of the sample were recorded in transmittance mode using a BaF, window and a 15×IR objective lens. Data processing was accomplished employing Opus [34].

The Raman spectrum was measured on an arbitrarily oriented single-crystal using a Horiba Jobin Yvon Labram-HR-800 spectrometer. A 532 nm frequencydoubled Nd:YAG laser, a 100× objective lens, a 100 μm slit, a 1000 µm pinhole and an optical grating with 1800 lines mm⁻¹ were used for the measurement. The excited area had a diameter of ~5 µm. An Andor CCD detector was employed to collect the scattered radiation in the wavenumber range 100-3700 cm⁻¹. Two spectra with an acquisition time of 150 s each were averaged using LABSPEC [35] (version 5.93.20). The baseline of the spectrum was fitted manually. Owing to strong fluorescence effects above 1500 cm⁻¹, the corresponding part of the Raman spectrum is not displayed in Fig. 6.

Acknowledgments: Special thanks go to G. Heymann for collecting the single-crystal diffraction data, D. Vitzthum

for the IR measurements, R. Stalder for granting us access to the FTIR-spectrometer, and B. Joachim for the Raman spectroscopic measurements.

References

- [1] M. Jansen, W. Scheld, Z. Anorg. Allg. Chem. 1981, 477, 85.
- [2] G. Brachtel, M. Jansen, Z. Anorg. Allg. Chem. 1981, 478, 13.
- [3] M. Jansen, G. Brachtel, Z. Anorg. Allg. Chem. 1982, 489, 42.
- [4] W. Depmeier, H. Schmid, Acta Crystallogr. 1982, B38, 605.
- [5] H. Huppertz, G. Heymann, *Solid State Sci.* **2003**, *5*, 281.
- [6] S. C. Neumair, J. S. Knyrim, O. Oeckler, R. Glaum, R. Kaindl, R. Stalder, H. Huppertz, Chem. Eur. J. 2010, 16, 13659.
- [7] G. Sohr, N. Ciaghi, K. Wurst, H. Huppertz, Z. Naturforsch. 2015, 70b, 183.
- [8] G. Sohr, N. Ciaghi, M. Schauperl, K. Wurst, K. R. Liedl, H. Huppertz, Angew. Chem. Int. Ed. 2015, 54, 6360.
- [9] M. K. Schmitt, O. Janka, R. Pöttgen, C. Benndorf, M. de Oliveira, H. Eckert, F. Pielnhofer, A.-S. Tragl, R. Weihrich, B. Joachim, D. Johrendt, H. Huppertz, Angew. Chem. Int. Ed. 2017, 56, 6449.
- [10] J. S. Knyrim, F. Roeßner, S. Jakob, D. Johrendt, I. Kinski, R. Glaum, H. Huppertz, Angew. Chem. Int. Ed. 2007, 46, 9097.
- [11] J. S. Knyrim, J. Friedrichs, S. Neumair, F. Roeßner, Y. Floredo, S. Jakob, D. Johrendt, R. Glaum, H. Huppertz, Solid State Sci. 2008, 10, 168.
- [12] M. K. Schmitt, O. Janka, O. Niehaus, T. Dresselhaus, R. Pöttgen, F. Pielnhofer, R. Weihrich, M. Krzhizhanovskaya, S. Filatov, R. Bubnova, L. Bayarjargal, B. Winkler, R. Glaum, H. Huppertz, Inorg. Chem. 2017, 56, 4217.
- [13] M. K. Schmitt, O. Janka, R. Pöttgen, K. Wurst, H. Huppertz, Eur. J. Inorg. Chem. 2017, 2017, 3508.

- [14] M. K. Schmitt, O. Janka, R. Pöttgen, H. Huppertz, Z. Anorg. Allg. Chem. DOI: 10.1002/zaac.201700130.
- [15] A. F. Holleman, N. Wiberg, E. Wiberg, Lehrbuch der Anorganischen Chemie, 102nd edition, De Gruyter, Berlin, 2007.
- [16] E. Zobetz, Z. Kristallogr. 1990, 191, 45.
- [17] E. Zobetz, Z. Kristallogr. 1982, 160, 81.
- [18] M. Pompetzki, B. Albert, Z. Anorg. Allg. Chem. 2004, 630, 2550.
- [19] T. Armbruster, G. A. Lager, J. Ihringer, F. J. Rotella, J. D. Jorgensen, Z. Kristallogr. 1983, 162, 8.
- [20] I. D. Brown, D. Altermatt, Acta Crystallogr. 1985, B41, 244.
- [21] N. E. Brese, M. O'Keeffe, Acta Crystallogr. 1991, B47, 192.
- [22] S. C. Neumair, R. Kaindl, H. Huppertz, J. Solid State Chem. 2012, 185, 1.
- [23] S. C. Neumair, S. Vanicek, R. Kaindl, D. M. Többens, K. Wurst, H. Huppertz, J. Solid State Chem. 2011, 184, 2490.
- [24] J. P. Laperches, P. Tarte, Spectrochim. Acta 1966, 22, 1201.
- [25] S. C. Neumair, S. Vanicek, R. Kaindl, D. M. Többens, C. Martineau, F. Taulelle, J. Senker, H. Huppertz, Eur. J. Inorg. Chem. 2011, 2011, 4147.
- [26] H. Huppertz, Z. Kristallogr. 2004, 219, 330.
- [27] D. Walker, Am. Mineral. 1991, 76, 1092.
- [28] D. Walker, M. A. Carpenter, C. M. Hitch, Am. Mineral. 1990, 75, 1020.
- [29] Z. Otwinowski, W. Minor in Methods in Enzymology, Vol. 276, Macromolecular Crystallography, Part A (Eds.: C. W. Carter Jr, R. M. Sweet), Academic Press, New York, 1997, pp. 307-326.
- [30] G. M. Sheldrick, Acta Crystallogr. 2015, C71, 3.
- [31] L. J. Farrugia, J. Appl. Crystallogr. 2012, 45, 849.
- [32] S. Parsons, H. D. Flack, T. Wagner, Acta Crystallogr. 2013, B69, 249.
- [33] TOPAS, Bruker AXS Inc., Madison, Wisconsin (USA) 2009.
- [34] Opus, Bruker, Billerica, Massachusetts (USA) 2008.
- [35] LABSPEC, Horiba Jobin Yvon GmbH, Bensheim (Germany) 2005.